Front. Phys. 13(5), 137204 (2018)
https://doi.org/10.1007/s11467-018-0800-4

RESEARCH ARTICLE

Efimov effect in Dirac semi-metals

Pengfei Zhang[1], **Hui Zhai**[1,2,†]

[1] *Institute for Advanced Study, Tsinghua University, Beijing 100084, China*
[2] *Collaborative Innovation Center of Quantum Matter, Beijing 100084, China*
Corresponding author. E-mail: [†]*huizhai.physics@gmail.com*
Received May 9, 2018; accepted May 22, 2018

The Efimov effect is defined as a quantum state with discrete scaling symmetry and a universal scaling factor. It has attracted considerable interests from nuclear to atomic physics communities. In a Dirac semi-metal, when an electron interacts with a static impurity through a Coulombic interaction, the same kinetic scaling and the interaction energy results in the Efimov effect. However, even when the Fermi energy lies exactly at the Dirac point, the vacuum polarization of the electron-hole pair fluctuation can still screen the Coulombic interaction, which leads to deviations from the scaling symmetry and eventually breaks down of the Efimov effect. This energy distortion of the Efimov states due to vacuum polarization is a relativistic electron analogy of the Lamb shift for the hydrogen atom. Motivated by the recent experimental observations in two- and three-dimensional Dirac semi-metals, we herein investigate this many-body correction to the Efimov effect and the conditions that allow some of the Efimov-like quasi-bound states to be observed in these condensed matter experiments.

Keywords Dirac semi-metal, Efimov effect, screening

PACS numbers 72.10.Fk

1 Introduction

The Efimov effect was first proposed by Vitaly Efimov in 1970 within a quantum three-boson system [1], where an infinite series of excited three-body energy levels exists when a two-body state is exactly at the dissociation threshold. To solve a three-body problem with a hyperspherical coordinate in the vicinity of a two-body resonance, the problem can be reduced to a one-dimensional Schrödinger equation given by

$$\left[-\frac{\hbar^2 \mathrm{d}^2}{2m\mathrm{d}^2 R}-\frac{(s_0^2+1/4)\hbar^2}{2mR^2}\right]\Psi = E\Psi. \quad (1)$$

The intriguing feature underlining Eq. (1) is the continuous scaling symmetry. The Schrödinger equation is still satisfied by rescaling $R \to \lambda R$ and $E \to E/\lambda^2$ with an arbitrary number λ. However, to prevent the Thomas collapse, one also has to impose a short-range boundary condition for the wave function, which in general breaks the scaling symmetry. The Efimov effect states that all eigenenergies of the bound states E_n form a geometric sequence and thus $E_n \exp(2\pi/s_0)$ is still an eigenenergy, where s_0 is a universal constant. This means that the solution with the boundary condition still exhibits a discrete scaling symmetry with a universal scaling factor. In the past decade, the Efimov effect has been observed and extensively studied in a number of few-body systems in cold atom systems [2–5], as well as in the helium trimer [6].

Here, we extend the definition of the "Efimov Effect" to a quantum state or a phenomenon with discrete scaling symmetry and a universal scaling factor, caused by a system with a continuous scaling symmetric Hamiltonian and a non-universal boundary condition. Two nontrivial points of this definition are worth highlighting. First, in most cases the boundary condition completely breaks the continuous scaling symmetry; however, in the Efimov effect, a discrete scaling symmetry remains. Next, despite the non-universality of the boundary condition, the scaling factor is still a universal constant that does not depend on the details of the boundary condition. With this general definition, the Efimov effect can be realized in many systems other than the few-body systems and can broadly impact areas beyond few-body physics. For instance, recently, the Efimovian expansion has been proposed and observed in the dynamics of many-body systems [7, 8].

In recent years, the studies of the Dirac and the Weyl semi-metals have received considerable attention in con-

*arXiv: 1711.03118.

densed matter physics [9–11]. In these systems, a linear dispersion for the electrons (or holes) is adopted. Therefore, if one considers a Coulombic interaction between an electron (or a hole) and a static impurity with opposite charge, the total Hamiltonian will possess a continuous scaling symmetry because the linear dispersion and the Coulombic interaction scale similarly. This is the reminiscent of Eq. (1) for the non-relativistic case. Similarly, a short-range boundary condition, depending on the details of the impurity, will break the continuous scaling symmetry down to a discrete one. This can results in the Efimov effect [12–15]. A recent experiment reported a log-periodic magnetoresistenance oscillation in a potential three-dimensional Dirac semi-metal $ZrTe_5$ [16]. They attributed this observation to the Efimov effect in the Dirac semi-metals [16]. Similar experimental evidence from local tunneling measurements near charged impurities has also been reported in graphene that can be regarded as a two-dimensional Dirac semi-metal [17]. To the best of our knowledge, these two are the first experimental manifestations of the Efimov effect in condensed matter systems.

However, in the considerations hitherto, the Coulombic interaction between electrons has been ignored. This Coulombic interaction can screen the interaction between electrons and impurity, and consequently distorts or even destroys the Efimov effect. We herein address the question: to what extent can the Efimov effect survive after the many-body interactions are included. Given the fact that such Coulombic interaction is undoubtedly present in the current experiments [16, 17], this question becomes critical for explaining these observations.

We begin with a simplified single Dirac point situation where the Fermi surface is right on the Dirac point and the electrons interact with a static impurity with charge Ze. Although the electron–hole pairs near the Dirac point are charge neutral, the electronic dipoles consisting of these pairs, i.e., the vacuum polarization, can still screen the potential between the electron and impurity, as schematized in Fig. 1(a). Thus, the behavior of the screened potential will no longer be proportional to $-1/r$, as schematically shown in Fig. 1(b) [18–20]. Subsequently, the screened potential loses the scale invariance. Moreover, because the shallow Efimov state is sensitive to the long-range part of the potential, these shallow quasi-bound states will first disappear when the screening effect appears.

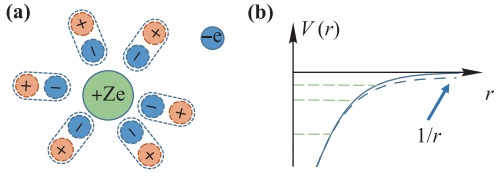

Fig. 1 **(a)** Schematic of the electron dipole screening of the interaction potential between an electron and the impurity. **(b)** Schematic of screened interaction potential with impurity and its effect on Efimov quasi-bound state.

This problem can be viewed as an analogy of the Lamb shift, where the vacuum polarization modifies the Coulombic potential between the electron and nucleus, which distorts the energy level of a hydrogen atom. However, a significant difference is noteworthy. Physically, for the Lamb shift, the electrons have a finite mass and are non-relativistic. In the Dirac or the Weyl semimetals, electrons with linear dispersions are essentially relativistic. Apparently, for the relativistic case, the energy level is more sensitive to the modification of the Coulombic potential. Technically, the traditional Lamb shift considers the shift in the energy of the bound state and directly computes the self-energy from radiation. In this manuscript, we will consider a quasi-bound state and use the Wilson renormalization scheme with certain diagrams.

2 Field theory model

To quantitatively address this issue, we employ the field theory approach. This is because, on the one hand, the Efimov effect can be captured by the limit cycle solutions of the renormalization group (RG). On the other hand, it is natural to include the screening effect owing to vacuum polarization. Thus, it provides a natural framework that combines both effects. By setting $v_{\mathrm{F}} = 1$, the Lagrangian for a Dirac semi-metal at $d = 3$ and $d = 2$ can be written as

$$\mathcal{L} = \int \mathrm{d}t\mathrm{d}^d\boldsymbol{r}\left[\bar{\psi}(\mathrm{i}\partial_\mu\gamma^\mu)\psi - \bar{\psi}\gamma^0\psi V(\boldsymbol{r}) - \mathrm{e}\bar{\psi}\gamma^0\psi\phi\right] + \mathcal{L}_\phi, \tag{2}$$

where $\mu = 0, 1, \ldots, d$. For $d = 3$, ψ is a four-component fermion field and

$$\gamma^\mu = \begin{pmatrix} 0 & \sigma^\mu \\ \bar{\sigma}^\mu & 0 \end{pmatrix}, \quad \sigma^\mu = (I, \boldsymbol{\sigma}), \quad \bar{\sigma}^\mu = (I, -\boldsymbol{\sigma}). \tag{3}$$

For $d = 2$, ψ is a two-component fermion field and $\gamma^0 = \sigma_z$, $\gamma^1 = i\sigma_y$, and $\gamma^2 = -i\sigma_x$. Thus, the first term results in a linear dispersion in d-dimension. In the second term, $V(\boldsymbol{r}) = -V_{\mathrm{c}}/|\boldsymbol{r}|$ is the Coulombic interaction between the electron and the static impurity at $\boldsymbol{r} = 0$ and $V_{\mathrm{c}} = Z\alpha$, and $e^2 = 4\pi\alpha$ at the bare level. ϕ describes the photon field mediating the instantaneous Coulombic interaction. The third term describes the coupling between the fermion and photon. The last term represents the Lagrangian for the photon field. For $d = 3$,

$$\mathcal{L}_\phi = \int \mathrm{d}t\mathrm{d}^3\boldsymbol{r}\frac{1}{2}(\nabla\phi)^2. \tag{4}$$

For $d = 2$, considering the following Fourier transformation

$$\int \mathrm{d}^2 r \frac{1}{r} \exp(\mathrm{i}\boldsymbol{q}\cdot\boldsymbol{r}) = \frac{2\pi}{|\boldsymbol{q}|}, \tag{5}$$

we have

$$\mathcal{L}_\phi = \int \mathrm{d}t \mathrm{d}^2\boldsymbol{q} |\boldsymbol{q}| \phi(\boldsymbol{q})\phi(-\boldsymbol{q}). \tag{6}$$

When the Efimov states exist, the wave function and the eigenenergy is sensitive to the short-range details. To include this effect, we should add an extra term in the effective field theory:

$$\mathcal{L}' = -\int \mathrm{d}t \mathrm{d}^d\boldsymbol{r} V_\mathrm{s} \bar{\psi}\gamma^0\psi\delta^d(\boldsymbol{r}). \tag{7}$$

V_s denotes the strength of this short-range interaction. In the RG analysis below, V_s flows as a function of the energy cutoff Λ. The energy scale Λ at which V_s diverges (or peaks) corresponds to the eigenenergy of the bound states (or quasi-bound states) [21]. A limit cycle behavior of this RG flow manifests the Efimov effect.

3 RG flow without screening effect

Before including the screening effect, we first turn off the coupling between the electron and photon, and review the formulation of the Efimov effect in this Coulombic impurity in term of RG flows as follows.

As shown in Fig. 2(a), defining the scattering amplitude between an electron and the impurity $M(\boldsymbol{k}', \boldsymbol{k}, E)$ where E is the energy, $\boldsymbol{k}$ is the incoming momenta and $\boldsymbol{k}'$ is the outgoing momenta; $M(\boldsymbol{k}', \boldsymbol{k}, E)$ satisfies a self-consistent equation that reads

$$\mathrm{i}M(\boldsymbol{k}', \boldsymbol{k}, E) = -\mathrm{i}V_1(\boldsymbol{k}', \boldsymbol{k})\gamma^0 + \int_0^\Lambda \frac{\mathrm{d}^3 q}{(2\pi)^3}(-\mathrm{i})V_1(\boldsymbol{q}, \boldsymbol{k})\mathrm{i}M(\boldsymbol{k}', \boldsymbol{q}, E)\frac{\mathrm{i}q_\mu\gamma^\mu}{E^2 - q^2 + \mathrm{i}\epsilon}\gamma^0, \tag{8}$$

where we define the one-particle irreducible scattering vertex:

$$V_1(\boldsymbol{k}', \boldsymbol{k}) = V_\mathrm{s} - \frac{4\pi V_\mathrm{c}}{(\boldsymbol{k} - \boldsymbol{k}')^2}. \tag{9}$$

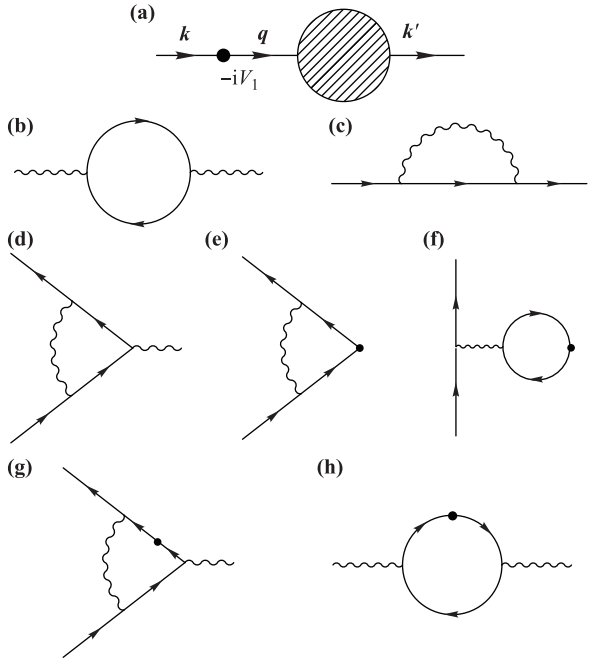

Fig. 2 **(a)** Diagram for scattering amplitude between electron and impurity. **(b, c)** Self-energy diagrams for photon (b) and for electron (c). **(d–f)** One-loop correction for single photon emission (d) and for single particle scattering vertex (e and f). **(g)** Diagram for single photon scattering. **(h)** Diagram for single photon emission with non-zero total momentum.

As the scattering amplitude is a physical observable, it should not depend on the high-energy cutoff Λ. Thus, we should choose V_s such that Eq. (8) results in a Λ-independent $M(\boldsymbol{k}', \boldsymbol{k}, E)$. With this requirement and following the strategy in Ref. [21], for $d = 3$, we obtain

$$\tilde{V}_\mathrm{s} = -4\pi V_\mathrm{c}\frac{\cos(s_0 \ln(\Lambda/\Lambda_0) + \phi)}{\cos(s_0 \ln(\Lambda/\Lambda_0) - \phi)}, \tag{10}$$

where $\tilde{V}_\mathrm{s} = V_\mathrm{s}\Lambda^2$, $s_0 = \sqrt{V_\mathrm{c}^2 - 1}$, $\tan\phi = s_0$, and Λ_0 is a fixed energy scale responsible for the non-universal short-range physics. Here, we have assumed the lifetime of the bound state is long without screening [12] and solved the self-consistent equation by disregarding the inhomogeneous term. This neglects the finite width of the quasi-bound states. For $d = 2$,

$$\tilde{V}_\mathrm{s} = -2\pi V_\mathrm{c}\frac{\cos(s_0 \ln(\Lambda/\Lambda_0) + \varphi)}{\cos(s_0 \ln(\Lambda/\Lambda_0) - \varphi)}, \tag{11}$$

where $\tilde{V}_\mathrm{s} = V_\mathrm{s}\Lambda$, $s_0 = \sqrt{V_c^2 - 1/4}$ and $\tan\varphi = 2s_0$. In both cases, $\tilde{V}_\mathrm{s}$ obtains a log-periodic structure, as shown in Fig. 3, and by scaling $\Lambda \to \mathrm{e}^{-n\pi/s_0}\Lambda$, $\tilde{V}_\mathrm{s}$ is invariant.

The renormalization relations of Eq. (10) and Eq. (11) can be used to derive an exact RG flow equation by requiring no explicit Λ-dependence on the r.h.s. of the RG equation:

$$\frac{\mathrm{d}\tilde{V}_\mathrm{s}}{\mathrm{d}\ln\Lambda} = 8\pi\frac{V_\mathrm{c}^2 - 1}{V_\mathrm{c}}\left\{1 + \frac{[4\pi(2 - V_\mathrm{c}^2) + \tilde{V}_\mathrm{s}V_\mathrm{c}]^2}{64\pi^2(V_\mathrm{c}^2 - 1)}\right\} \tag{12}$$

for $d = 3$ and

$$\frac{\mathrm{d}\tilde{V}_\mathrm{s}}{\mathrm{d}\ln\Lambda}=2\pi s_0 V_\mathrm{c}\sin(2\varphi)\times\left\{\frac{[2\pi V_\mathrm{c}(1-4s_0^2)+\tilde{V}_\mathrm{s}(1+4s_0^2)]^2}{64\pi^2 s_0^2 V_\mathrm{c}^2}+1\right\} \tag{13}$$

for $d=2$. It can be easily shown that the solution of Eq. (12) and Eq. (13) reproduce Eq. (10) and Eq. (11), respectively.

4 RG flow with screening effect

We now discuss the coupling between the electron and photon. The strategy is to treat the interaction between the electron and impurity exactly as discussed above, while the interaction between the electron and photon is treated perturbatively. As the RG equation should recover to the exact one when the electron–photon coupling is deactivated, we can therefore add the diagram from the perturbative calculation onto the exact RG equation derived above.

The principles for selecting the diagrams for the electron–photon interaction are listed as follows: (i) In the Wilson renormalization group calculation, because we only performed the momentum integration over a thin shell with width $\mathrm{d}\Lambda$ at energy Λ at each step, thus, to the order of $O(\mathrm{d}\Lambda/\Lambda)$, we only considered the one-loop diagrams for the irreducible self-energy or vertex, which only contains a single momentum integral. This selects the diagrams shown in Figs. 2(b)–(g). (ii) We only retain the diagrams that are relevant or marginal for power counting. These diagrams are critical in the low-energy limit. Consequently, diagram (g) that describes the emission of a photon with non-zero total momentum can be neglected. Because to the one-loop order and for a small total momentum, diagram (g) results in

$$\int \mathrm{d}t\mathrm{d}\boldsymbol{p}_1\mathrm{d}\boldsymbol{p}_2 d\boldsymbol{p}_3\phi(\boldsymbol{p}_1)\bar{\psi}(\boldsymbol{p}_2)\gamma^0\psi(\boldsymbol{p}_3)\frac{e'}{(\boldsymbol{p}_3+\boldsymbol{p}_1-\boldsymbol{p}_2)^2}, \tag{14}$$

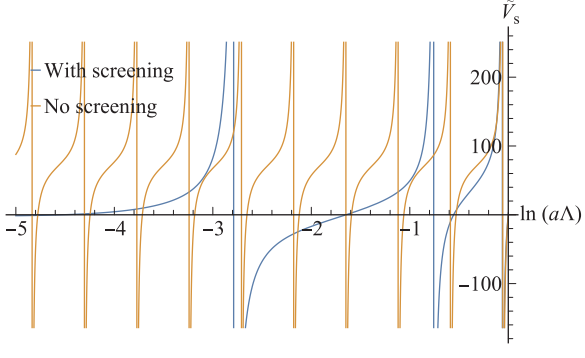

Fig. 3 A typical flow diagram for $\tilde{V}_\mathrm{s}$ for the case without screening effect (yellow dashed line) and for the case with screening effect (blue solid line). Here $d=3$, $Z=2$ and $\alpha=3$.

which is irrelevant. (iii) Diagram (h) represents the single-body scattering of photon, and is indeed zero as it is equal to a three-photon scattering diagram that vanishes owing to the particle–hole symmetry. Hence, we only need to include the contribution of (b–f) in the Fig. 2.

By considering these diagrams and following the standard Wilson RG procedure [22], one arrives at the following RG flow equations for $d=3$:

$$\frac{\mathrm{d}\tilde{V}_\mathrm{s}}{\mathrm{d}\ln\Lambda}=\text{r.h.s. of Eq. (12)}+\frac{V_\mathrm{c}e^2}{6\pi}+\frac{2\tilde{V}_\mathrm{s}e^2}{3\pi^2}, \tag{15}$$

$$\frac{\mathrm{d}V_\mathrm{c}}{\mathrm{d}\ln\Lambda}=\frac{V_\mathrm{c}e^2}{3\pi^2}, \tag{16}$$

$$\frac{\mathrm{d}e}{\mathrm{d}\ln\Lambda}=\frac{e^3}{6\pi^2}. \tag{17}$$

Here, we choose the initial condition for the RG flow starting at the momentum scale $\Lambda\sim 1/a$, where a is treated as the lattice energy length, at which the bare value $V_\mathrm{c}(1/a)=Z\alpha$, $\tilde{V}_\mathrm{s}(1/a)=0$, $e(1/a)=\sqrt{4\pi\alpha}\equiv e_0$, and $\tilde{V}_\mathrm{s}(1/a)=0$. One can solve the last two equations analytically:

$$e^2(\Lambda)=\frac{e_0^2}{1-e_0^2\ln(\Lambda a)/(3\pi^2)}, \tag{18}$$

$$V_c(\Lambda)=\frac{Z\alpha}{1-e_0^2\ln(\Lambda a)/(3\pi^2)}. \tag{19}$$

This originates from two effects. First, although the zero density of states near the Fermi surface leads to an infinite screening length, a $\ln r$ screening should still occur for the Coulombic potential owing to the particle–hole excitations. Next, the Fermi velocity actually flows under the RG; however, because we set $v_F=1$, V_0 becomes smaller.

As shown in Fig. 3, because of the extra terms in Eq. (15), the limit cycle solution is destroyed after a few periods. Moreover, the decrease in V_0 by lowering Λ yields a larger periodicity because $s_0(\Lambda)\sim\sqrt{V_0^2(\Lambda)-1}$. The energies of the quasi-bound state no longer obey the perfect geometric sequence.

Similarly, for $d=2$:

$$\frac{\mathrm{d}\tilde{V}_\mathrm{s}}{\mathrm{d}\ln\Lambda}=\text{r.h.s. of Eq. (13)}+\frac{e^2\tilde{V}_\mathrm{s}}{8\pi}, \tag{20}$$

with

$$e^2(\Lambda)=\frac{e_0^2}{1-e_0^2\ln(\Lambda a)/(16\pi)}, \tag{21}$$

$$V_c(\Lambda) = \frac{Z\alpha}{1 - e_0^2 \ln(\Lambda a)/(16\pi)}, \tag{22}$$

where the only correction comes from diagram (c) in Fig. 2, which renormalizes the Fermi velocity. All the other diagrams provide a correction on the order of $\boldsymbol{q}^2$ at low energies, which is smaller compared to the $|\boldsymbol{q}|$ behavior of the photon propagator and the impurity vertex, or the constant coupling of a single photon emission.

The final results of this work are presented in Fig. 4 and Fig. 5 for $d = 3$ and $d = 2$ Dirac semi-metals, respectively. Essentially, Z and α are the only two parameters in these systems. In Fig. 4(a) and Fig. 5(a), we show the number of quasi-bound states for various Z and α, respectively. In Fig. 4(b) and Fig. 5(b), we show the extents to which the quasi-bound state energies obey a geometric sequence. It is evident that in both cases, the larger the Z, the more stable is the Efimov effect. This can be crudely understood as that the correction to V_c is controlled by $e_0^2 \ln(E_n a) \sim e_0^2/s_0 \sim 1/Z$, and this correction is smaller for a larger Z. In the experiment of Ref. [16] from a three-dimensional Dirac semi-metal, approximately five logarithmic periods have been observed in the magnetoresistance oscillation. Our results suggest that a larger Z is required to attain such a regime and the experimental observation is more likely due to a static impurity with a large charge in the material.

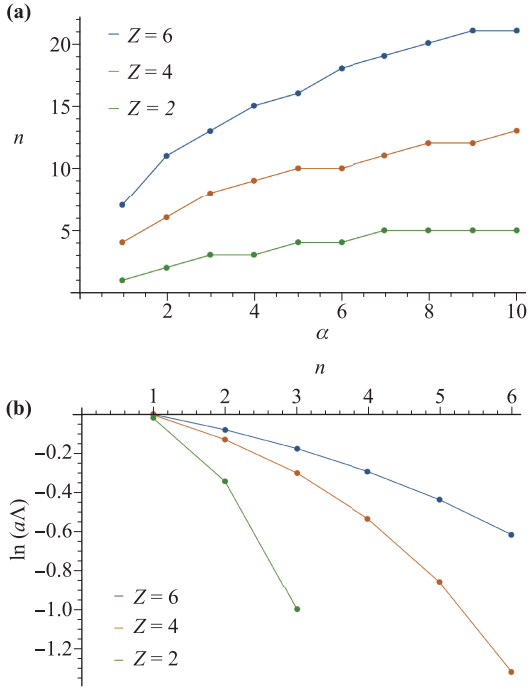

Fig. 4 Dirac semi-metal at $d = 3$. **(a)** The number of quasi-bound state vs. α for three different values of Z. **(b)** The bound state energy E_n, plotted in a dimensionless form $\ln(aE_n)$, for different n and with three different values of Z. α is fixed at $\alpha = 5$.

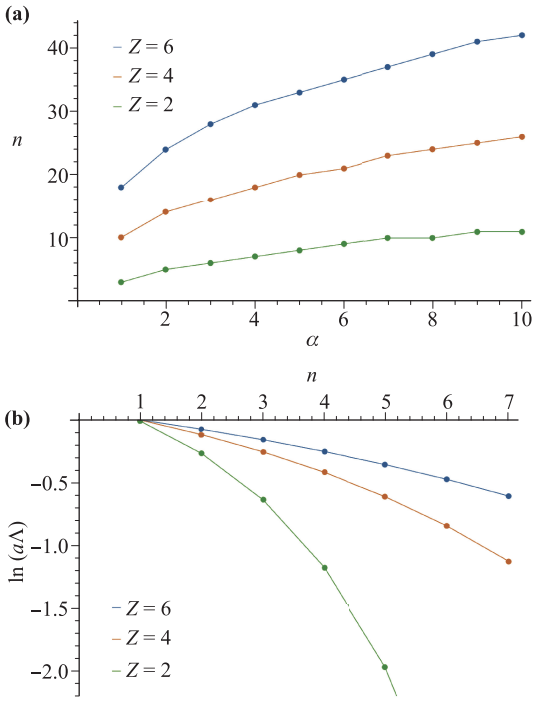

Fig. 5 The same plot as Fig. 4 but for $d = 2$ Dirac semi-metal. Here α is also fixed at $\alpha = 5$.

5 summary

In conclusion, we have studied the many-body correction of vacuum polarization based on the Efimov effect between a Dirac electron and a charged impurity, which is an analogy of the Lamb shift for "relativistic hydrogen atoms". Our results are directly related to the recent transport experiments on Dirac materials, and can also be applied to Weyl materials. This paves the way toward a more solid understanding of the emergent Efimov effect in condensed matter systems.

Acknowledgements We would like to thank Hong Yao, Ran Qi, Jian Wang and Haiwen Liu for helpful discussion. We thank Juan Yao for carefully reading the manuscript and giving advises for presentation. This work was supported by MOST under Grant No. 2016YFA0301600 and NSFC under Grant Nos. 11325418 and 11734010.

Appendix A Derivation of perturbative RG equations

In this appendix, we outline the calculation that leads to the renormalization relations (15), (16) and (17) for Dirac fermions for $d = 3$. The calculation for $d = 2$ is similar. We choose to employ a perturbative Wilson RG

scheme with a cutoff Λ in momentum space. In other words, the integration over momentum $\boldsymbol{q}$ is performed over a momentum shell $\Lambda - \mathrm{d}\Lambda < |\boldsymbol{q}| < \Lambda$ while the frequency is integrated from $-\infty$ to ∞. The diagrams we considered are shown in Fig. 2 as explained in the main text.

Before integrating out the high-energy fluctuation, we have an action at cut-off Λ:

$$S^{(\Lambda)} = \int \mathrm{d}^3x\mathrm{d}t \left[\bar{\psi}(\mathrm{i}\partial_\mu\gamma^\mu)\psi + \bar{\psi}\gamma^0\psi V_c(\Lambda)/|\boldsymbol{r}| - e(\Lambda)\bar{\psi}\gamma^0\psi\phi + \frac{1}{2}(\nabla\phi)^2 - V_s(\Lambda)\bar{\psi}\gamma^0\psi\delta^{(3)}(\boldsymbol{x})\right]. \tag{A1}$$

After integrating out the virtual particles in the moementum shell and performing a rescaling, we could derive the effective action defined with cutoff $\Lambda - \mathrm{d}\Lambda$. Then we find the RG equations for $\tilde{V}_s$, V_c and e by comparing it with the definition of $S^{(\Lambda-\mathrm{d}\Lambda)}$.

Firstly we need to include the renormalization of photon propagator. This is given by the self energy $\Pi(\omega, \boldsymbol{p})$ of photons as shown in the diagram in Fig. 2(b). Using the Feynman rules, we have

$$\begin{aligned}\mathrm{i}\Pi(\omega,\boldsymbol{p}) &= -\int \frac{\mathrm{d}^4q}{(2\pi)^4} e^2 \frac{\mathrm{tr}\left[\gamma^0\gamma^\mu\gamma^0\gamma^\nu\right]}{(\omega+q_0)^2-(\boldsymbol{p}+\boldsymbol{q})^2+\mathrm{i}\epsilon}\frac{(p+q)_\mu q_\nu}{(q_0)^2-(\boldsymbol{q})^2+\mathrm{i}\epsilon} \\ &= -\int \frac{\mathrm{d}^4q}{(2\pi)^4}\frac{(\omega+q_0)q_0+(\boldsymbol{p}+\boldsymbol{q})\cdot\boldsymbol{q}}{(\omega+q_0)^2-(\boldsymbol{p}+\boldsymbol{q})^2+\mathrm{i}\epsilon}\frac{4e^2}{(q_0)^2-(\boldsymbol{q})^2+\mathrm{i}\epsilon}.\end{aligned} \tag{A2}$$

We keep the leading order contribution for small ω and $\boldsymbol{p}$ by the Taylor expansion. Firstly we set $\boldsymbol{p} = 0$ and this gives the result

$$\begin{aligned}\mathrm{i}\Pi(\omega,\boldsymbol{0}) \propto \int \mathrm{d}^3q \Bigg\{ &\frac{-q(-q-\omega)+q^2}{[(q+\omega)^2-q^2](-2q)} \\ &+\frac{-q(-q+\omega)+q^2}{[(-q+\omega)^2-q^2](-2q)}\Bigg\} = 0.\end{aligned} \tag{A3}$$

after integrating out q_0 using contour integral. This means we only have terms proportional to $\boldsymbol{p}^2$, which gives the field strength renormalization for ϕ. Thus we set $\omega = 0$, and expand $\Pi(0, \boldsymbol{p})$ to the order of $\boldsymbol{p}^2$:

$$\begin{aligned}\mathrm{i}\Pi(0,\boldsymbol{p}) &= -\int \frac{\mathrm{d}^4q}{(2\pi)^4}\frac{q_0^2+(\boldsymbol{p}+\boldsymbol{q})\cdot\boldsymbol{q}}{q_0^2-(\boldsymbol{p}+\boldsymbol{q})^2+\mathrm{i}\epsilon}\frac{4e^2}{q_0^2-(\boldsymbol{q})^2+\mathrm{i}\epsilon} \\ &= \mathrm{i}\frac{e^2}{6\pi^2}\boldsymbol{p}^2\mathrm{d}\ln\Lambda.\end{aligned} \tag{A4}$$

The contribution to the renormalization of the single-particle scattering vertex shown diagram in Fig. 2(f) indeed gives the same result. Another contribution to the single-particle scattering is given by diagram (e), this gives

$$\mathrm{i}M_s(0,\boldsymbol{k})\left(\mathrm{i}\frac{4\pi V_c}{k^2}-\mathrm{i}V_s\right) = \int \frac{\mathrm{d}^4q}{(2\pi)^4}(-\mathrm{i}e\gamma^0)\frac{\mathrm{i}(q+k)_\mu\gamma^\mu}{(q+k)_\mu(q+k)^\mu}\gamma^0\frac{\mathrm{i}q_\mu\gamma^\mu}{q_\mu q^\mu}(-\mathrm{i}e\gamma^0)\left(\mathrm{i}\frac{4\pi V_c}{k^2}-\mathrm{i}V_s\right)\frac{\mathrm{i}}{\boldsymbol{q}^2}. \tag{A5}$$

Here we define $k_\mu = (0, \boldsymbol{k})$ and $k = |\boldsymbol{k}|$. After expanding to the lowest order of k, we find the result is

$$\left(\mathrm{i}\frac{4\pi V_c}{k^2}-\mathrm{i}V_s\right)\frac{e^2k^2}{24\pi^2}. \tag{A6}$$

The renormalization of the photon emission vertex is shown in Fig. 2(d). Expanding to the zero-th order of frequency and momentum, it is just given by $\mathrm{i}M_s(0, \boldsymbol{0}) = 0$.

At last we consider the self energy $D(\omega, \boldsymbol{k})$ shown in Fig. 2(c). This diagram renormalizes propagator for the fermion as $\mathrm{i}/(k_\mu\gamma^\mu - D)$:

$$-\mathrm{i}D(\omega,\boldsymbol{k}) = \int \frac{\mathrm{d}^4q}{(2\pi)^4}\frac{e^2}{\boldsymbol{q}^2}\frac{q_0 I-(q+k)^i\gamma^i}{q_0^2-(\boldsymbol{q}+\boldsymbol{k})^2+\mathrm{i}\epsilon}. \tag{A7}$$

There is no ω dependence, and the constant part is indeed non-physical which should be canceled by tuning the chemical potential. We only consider the momentum dependent part and find

$$-\mathrm{i}(D(\omega,\boldsymbol{k})-D(\omega,\boldsymbol{0})) = k_i\gamma^i\frac{\mathrm{i}e^2}{6\pi^2}\mathrm{d}\ln\Lambda. \tag{A8}$$

Adding all these contributions together, we find the effective action after integrating out virtual particles:

$$\begin{aligned}S_{\mathrm{eff}}^{(\Lambda-\mathrm{d}\Lambda)} = &\int \mathrm{d}^3x\mathrm{d}t\bar{\psi}\left[\mathrm{i}\partial_0\gamma^0+\mathrm{i}\partial_i\gamma^i\left(1+\frac{e^2}{6\pi^2}\mathrm{d}\ln\Lambda\right)\right]\psi \\ &+\bar{\psi}\gamma^0\psi\frac{V_c(\Lambda)}{\left(1+\frac{e^2}{6\pi^2}\mathrm{d}\ln\Lambda\right)|\boldsymbol{x}|}\end{aligned}$$

$$-e(\Lambda)\bar{\psi}\gamma^0\psi\phi+\frac{1}{2}\left(1+\frac{e^2}{6\pi^2}\mathrm{d}\ln\Lambda\right)(\nabla\phi)^2$$
$$-V_s(\Lambda)\frac{1-\frac{V_c e^2}{6\pi}\mathrm{d}\ln\Lambda}{1+\frac{e^2}{6\pi^2}\mathrm{d}\ln\Lambda}\bar{\psi}\gamma^0\psi\delta^{(3)}(\boldsymbol{x}). \quad \text{(A9)}$$

To bring it back to the form of $S^{(\Lambda-\mathrm{d}\Lambda)}$, we rescale $x\to\left(1+\frac{e^2}{6\pi^2}\mathrm{d}\ln\Lambda\right)x$, $\psi\to\left(1+\frac{e^2}{6\pi^2}\mathrm{d}\ln\Lambda\right)^{-3/2}\psi$ and $\phi\to\left(1+\frac{e^2}{6\pi^2}\mathrm{d}\ln\Lambda\right)^{-1}\phi$. Finally, we find the renormalization relations:

$$\frac{\mathrm{d}\tilde{V}_s}{\mathrm{d}\ln\Lambda}=8\pi\frac{V_c^2-1}{V_c}\left\{1+\frac{[4\pi(2-V_c^2)+\tilde{V}_sV_c]^2}{64\pi^2(V_c^2-1)}\right\}+\frac{V_ce^2}{6\pi}+\frac{2\tilde{V}_se^2}{3\pi^2}, \quad \text{(A10)}$$

$$\frac{\mathrm{d}V_c}{\mathrm{d}\ln\Lambda}=\frac{V_ce^2}{3\pi^2},\quad \frac{\mathrm{d}e}{\mathrm{d}\ln\Lambda}=\frac{e^3}{6\pi^2}. \quad \text{(A11)}$$

References and notes

1. V. Efimov, Energy levels arising from resonant two-body forces in a three-body system, *Phys. Lett. B* 33(8), 563 (1970)
2. T. Kraemer, M. Mark, P. Waldburger, J. G. Danzl, C. Chin, B. Engeser, A. D. Lange, K. Pilch, A. Jaakkola, H. C. Nägerl, and R. Grimm, Evidence for Efimov quantum states in an ultracold gas of caesium atoms, *Nature* 440(7082), 315 (2006)
3. B. Huang, L. A. Sidorenkov, R. Grimm, and J. M. Hutson, Observation of the second triatomic resonance in Efimov's scenario, *Phys. Rev. Lett.* 112(19), 190401 (2014)
4. R. Pires, J. Ulmanis, S. Häfner, M. Repp, A. Arias, E. D. Kuhnle, and M. Weidemüller, Observation of Efimov resonances in a mixture with extreme mass imbalance, *Phys. Rev. Lett.* 112(25), 250404 (2014)
5. S. K. Tung, K. Jiménez-García, J. Johansen, C. V. Parker, and C. Chin, Geometric scaling of Efimov states in a ^{6}Li-^{133}Cs mixture, *Phys. Rev. Lett.* 113(24), 240402 (2014)
6. M. Kunitski, S. Zeller, J. Voigtsberger, A. Kalinin, L. P. H. Schmidt, M. Schoffler, A. Czasch, W. Schollkopf, R. E. Grisenti, T. Jahnke, D. Blume, and R. Dorner, Observation of the Efimov state of the helium trimer, *Science* 348(6234), 551 (2015)
7. S. Deng, Z. Y. Shi, P. Diao, Q. Yu, H. Zhai, R. Qi, and H. Wu, Observation of the Efimovian expansion in scale-invariant Fermi gases, *Science* 353(6297), 371 (2016)
8. Z.-Y. Shi, R. Qi, H. Zhai, Z. Yu, Dynamic super Efimov effect, *Phys. Rev. A* 96, 050702(R) (2017)
9. A. H. Castro Neto, F. Guinea, N. M. R. Peres, K. S. Novoselov, and A. K. Geim, The electronic properties of graphene, *Rev. Mod. Phys.* 81(1), 109 (2009)
10. M. Z. Hasan and C. L. Kane, Topological insulators, *Rev. Mod. Phys.* 82(4), 3045 (2010)
11. X. L. Qi and S. C. Zhang, Topological insulators and superconductors, *Rev. Mod. Phys.* 83(4), 1057 (2011)
12. A. V. Shytov, M. I. Katsnelson, and L. S. Levitov, Atomic collapse and quasi-Rydberg states in graphene, *Phys. Rev. Lett.* 99(24), 246802 (2007)
13. V. M. Pereira, J. Nilsson, and A. H. C. Neto, Coulomb impurity problem in graphene, *Phys. Rev. Lett.* 99(16), 166802 (2007)
14. Y. Nishida, Vacuum polarization of graphene with a supercritical Coulomb impurity: Low-energy universality and discrete scale invariance, *Phys. Rev. B* 90(16), 165414 (2014)
15. Y. Nishida, Renormalization group analysis of graphene with a supercritical Coulomb impurity, *Phys. Rev. B* 94(8), 085430 (2016)
16. H. Wang, H. Liu, Y. Li, Y. Liu, J. Wang, J. Liu, Y. Wang, L. Li, J. Yan, D. Mandrus, X. C. Xie, and J. Wang, Discrete scale invariance and fermionic Efimov states in ultra-quantum $ZrTe_5$, arXiv: 1704.00995
17. O. Ovdat, J. Mao, Y. Jiang, E. Y. Andrei, and E. Akkermans, Observing a scale anomaly and a universal quantum phase transition in graphene, *Nat. Commun.* 8(1), 507 (2017)
18. A. V. Shytov, M. I. Katsnelson, and L. S. Levitov, Vacuum polarization and screening of supercritical impurities in graphene, *Phys. Rev. Lett.* 99(23), 236801 (2007)
19. H. Isobe and N. Nagaosa, Theory of a quantum critical phenomenon in a topological insulator: (3 + 1)-dimensional quantum electrodynamics in solids, *Phys. Rev. B* 86(16), 165127 (2012)
20. S. K. Jian and H. Yao, Correlated double-Weyl semimetals with Coulomb interactions: Possible applications to $HgCr_2Se_4$ and $SrSi_2$, *Phys. Rev. B* 92(4), 045121 (2015)
21. E. Braaten and H. W. Hammer, Universality in few-body systems with large scattering length, *Phys. Rep.* 428(5–6), 259 (2006)
22. See Appendix A for detailed derivation.